

ARPD: Anchor-free Rotation-aware People Detection using Topview Fisheye Camera

Quan Nguyen Minh ^{1,2}, Bang Le Van ², Can Nguyen ², Anh Le ³ and Viet Dung Nguyen ¹

¹ Hanoi University of Science and Technology
dung.nguyenviet1@hust.edu.vn

² Viettel High Technology Industries Corporation
{quannm23,banglv1,cannn1}@viettel.com.vn

³ FPT University
anhldhe130082@fpt.edu.vn

Abstract

People detection in top-view, fish-eye images is challenging as people in fish-eye images often appear in arbitrary directions and are distorted differently. Due to this unique radial geometry, axis-aligned people detectors often work poorly on fish-eye frames. Recent works account for this variability by modifying existing anchor-based detectors or relying on complex pre/post-processing. Anchor-based methods spread a set of pre-defined bounding boxes on the input image, most of which are invalid. In addition to being inefficient, this approach could lead to a significant imbalance between the positive and negative anchor boxes. In this work, we propose ARPD, a single-stage anchor-free fully convolutional network to detect arbitrarily rotated people in fish-eye images. Our network uses keypoint estimation to find the center point of each object and regress the object's other properties directly. To capture the various orientation of people in fish-eye cameras, in addition to the center and size, ARPD also predicts the angle of each bounding box. We also propose a periodic loss function that accounts for angle periodicity and relieves the difficulty of learning small-angle oscillations. Experimental results show that our method competes favorably with state-of-the-art algorithms while running significantly faster.

I. Introduction

Omni-directional cameras, most notably fish-eye cameras, are widely used for surveillance applications. One top-view fish-eye camera covers the same area as many conventional perspective cameras due to their 360° field

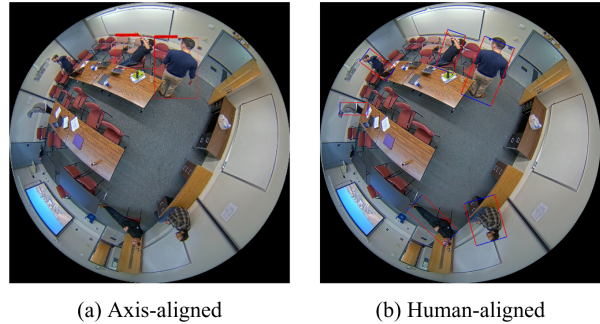


Fig. 1. Illustration of typical people-detection results on ceiling-mounted, fish-eye images of conventional person detector (a) and the proposed method (b). Human-aligned bounding boxes fit bodies more accurately compared to axis-aligned bounding boxes.

of view. Another advantage of a ceiling-mounted fish-eye camera is minimal occlusion between objects in a frame. However, images from overhead-mounted fish-eye cameras may have human bodies at various orientations and poses. Another difficulty is severe geometric distortions at the peripheral areas of a fish-eye image, which can cause an object's appearance to varying. Pedestrian detectors trained with perspective images [1], [2], [3] cannot accommodate these variations and deformations, hence do not work well on top-view fish-eye images, often missing non-up-right bodies. (Fig. 1a)

Various methods have been proposed to tackle these problems. In early works, features are extracted using rudimentary methods such as background subtraction or edge detection [4], [5]. These features have poor discrimination power and are sensitive to environmental changes

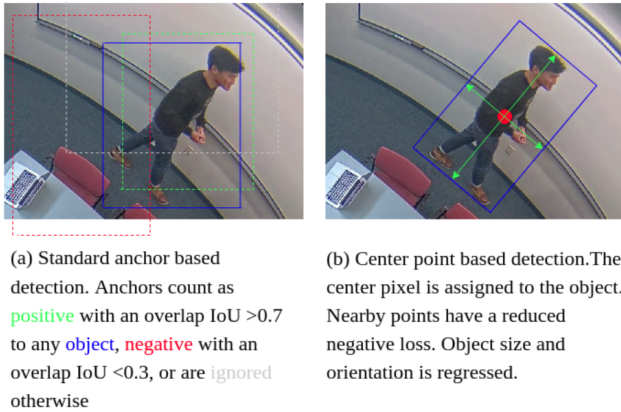


Fig. 2. Difference between anchor-based detectors (a) and our center point detector (b). Best viewed in color. As horizontal proposals are located along the image edge, the extracted feature of an object may contain features of background and nearby objects.

and noise. Another approach utilizes traditional person detectors such as HOG and LBP, making slight adjustments to accommodate fish-eye geometry [6], [7], [8]. Recently, CNN-based people detection methods have been proposed for over-head, fish-eye images [9], [10], [11]. To deal with the radial geometry, these works often require complex pre-/post processing. For example, Li *et al.* [9] applied YOLOv3 [1] to 24 rotated, overlapping windows, and the results are re-mapped to the original image. However, this requires YOLOv3 to run 24 times for each frame. Tamura *et al.* [10] tries to train a rotation-invariant model by introducing rotation augmentation during training. RAPiD [11] modifies YOLOv3 to detect people in fish-eye images using oriented bounding boxes. However, applying horizontal-anchor-based detectors such as YOLOv3 or Faster-RCNN [3] to the oriented object detection task would lead to misalignment between the extracted features and object’s features (Fig. 2a). A straightforward way to deal with this problem is to use oriented anchor boxes [12], [13], [14]. However, rotated anchors need to take the predefined angle (or orientation of object) into account. Hence, the number of anchors can be dramatically increased, increasing computational cost. Furthermore, the vast imbalance between the positive and negative anchors would lead to slow training and inferior performance. [15]

In this paper, we propose ARPD, a novel single-stage anchor-free convolutional neural network that detects arbitrarily rotated bounding boxes of people in top-view fish-eye images. Our work extends the model proposed in CenterNet [16], one of the novel keypoint-based object detection algorithms [17], [18], [16] for standard images. We model each object as the center point of its bounding

box. Other properties are directly inferred from the center keypoint feature. To capture the various alignment of people in ceiling-mounted fish-eye images, we predict the angle of each bounding box in addition to center and size. We also introduce a new rotation-aware periodic loss function that takes into account angle periodicity. The addition of an orientation head and a novel angle loss function allows ARPD to directly infer the oriented bounding boxes in fish-eye images without the need for prior boxes or non-maximal suppression. We evaluate the performance of ARPD on three publicly available person detection datasets captured by ceiling-mounted fish-eye cameras: HABBOF [9], Mirror World [19] and CEPDOF [11]. The main contributions of this paper can be summarized as follows:

- We propose ARPD, a single-stage anchor-free detector for rotation-aware people detection in overhead fish-eye images. Our method eliminates the need for multiple anchors and complex pre/post-processing. In experiments on multiple fish-eye datasets, ARPD achieved competitive performance compared to state-of-the-art methods and keeps a real-time inference speed.
- We introduce a periodic loss function that allows our network to learn the symmetry of rotated people in top-view fish-eye images. Our loss function does not suffer from the training instability and performance degeneration caused by the loss discontinuity when using standard regression functions.

II. Related Works

Horizontal object detection: Horizontal object detectors can be roughly classified into two categories: anchor-based and keypoint-based. The former consists of two-stage and one-stage methods. Two-stage detectors, most notably models from the R-CNN family [21], [3], [22] are region-based. First, the model proposes a set of regions of interest. Then a classifier only processes the region candidates. One-stage detectors such as YOLOv3 [1] or SSD [2] skips the region proposal stage and runs detection directly over a dense sampling of possible locations, known as anchor boxes. Recently, keypoint-based detectors have been proposed to overcome the disadvantages of anchor-based solutions. CornerNet [17] predicts the upper-left and lower-right corners of bounding boxes for every pixel along with an embedding, which is then used to determine the objects. ExtremeNet [18] predicts the center of objects as well as farthest left, right, top, and bottom points. These points are then matched based on their geometry. However, the post-grouping process is time-consuming. Zhou’s CenterNet [16] considers the center of a box as an object as well as a key point and then uses this predicted center to find the coordinates/offsets of the bounding box

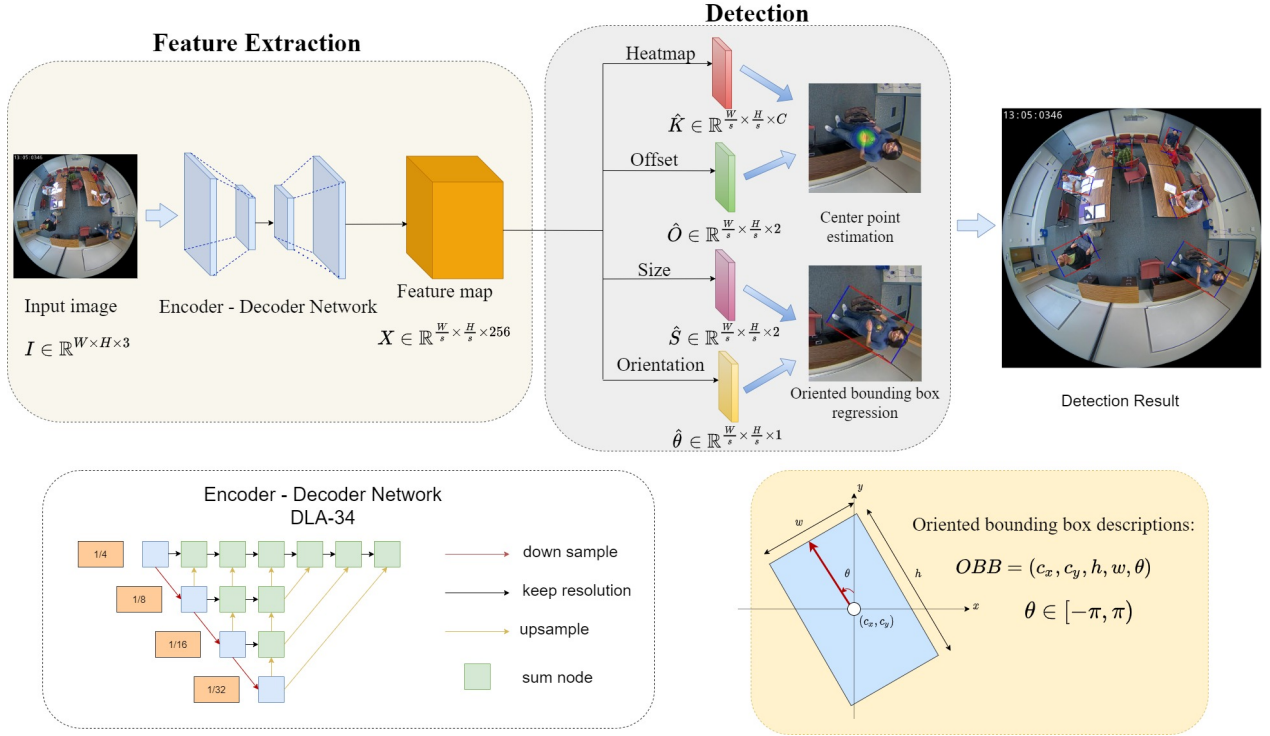


Fig. 3. The overall architecture and the oriented bounding box (OBB) descriptions of the proposed method. We use a modified version of DLA-34 [20] as the encoder-decoder network as it gives the best speed and accuracy tradeoff [16]. We replace the upsampling layers with 3x3 deformable convolution layers and add more skip connections from the lower layers to help increase the feature map resolution symmetrically. The output feature map is transformed into four branches: heatmap, off-set, size, and orientation. In addition to center point and size, the OBB is also represented by its angle of rotation.

without post-grouping, thus making prediction faster. The keypoint-based object detectors show advantages over the anchor-based ones in terms of speed and accuracy. [16]

Oriented Object Detection: Different from horizontal object detectors, these algorithms use rotated bounding boxes to represent oriented objects. R-DFPN [12] designs a rotation anchor strategy to predict the minimum circumscribed rectangle of the object and build dense connections to create high-level semantic feature maps for all scales. RoI Transformer [13] designed a Rotated RoI learner to transform a Horizontal Region of Interest into a Rotated Region of Interest. To solve the misalignment problems between the region of interest and the object's feature, R3Det [14] proposes an end-to-end refined single-stage rotated object detector. All of the methods above use five parameter coordinates to describe oriented bounding box: center, width, height and rotation angle, with the angle defined in $[-\frac{\pi}{2}, 0]$ and use common regression loss. However, due to the inherent symmetry of rotated bounding boxes, this approach will lead to loss discontinuity (i.e., loss value will jump when the angle reaches its range boundary) and instability during training.

People detection using overhead, fish-eye cameras:

Person detection methods using ceiling-mounted fish-eye cameras have been much less studied than conventional algorithms using standard perspective cameras, with most research appearing in recent years. Early works use techniques such as background subtraction or optical flow to obtain the location of moving people [5], [4]. Methods based on Histogram of Gradients (HOG) or Local Binary Patterns (LBP) [6], [8], [7] have also been put forward. Chiang and Wang [7] applied HOG descriptor with SVM classifier on sections sliding windows extracted from fish-eye frames. In a recent work, instead of directly de-warping the fish-eye images, Krams *et al.* [8] de-warp features extracted from the fish-eye image using an ACF classifier.

Recently, deep learning-based algorithms have been applied to person detection in fish-eye images [9], [11], [10]. Li *et al.* [9] proposes a method in which YOLOv3 is applied to 24 rotated, overlapping windows, and the results are post-processed to produce detection results. One of the top-performing algorithms, RAPID [11] propose a

fully convolutional network also based on YOLOv3 that detects people in fish-eye images using rotated bounding boxes. All of the methods mentioned above either require excessive computation or make modifications to horizontal anchor-based detectors, which are prone to feature misalignment problems as well as severe imbalance issues.

III. Proposed Method

We propose ARPD, a novel single-stage anchor-free CNN that extends Zhou’s CenterNet [16]. Unlike Centernet which only predicts the location and size of each object, ARPD also predicts the angle of bounding boxes of people in a top-down, fish-eye image. We also introduce a periodic loss function based on an extension of common smooth L1 loss to deal with the loss discontinuity caused by angle periodicity.

In this section, we first describe the overall architecture of the proposed method and the output maps in detail. The results of the output maps are then gathered and decoded to determine the center-point, size, and orientation of each person in an overhead fish-eye image.

A. Network Architecture

The proposed network (see Fig. 3) consists of a feature extraction network and a bounding box regression network, also known as detection head. The feature extraction network takes an image $I \in \mathbb{R}^{W \times H \times 3}$ as input and returns an output feature map. The output feature map $X \in \mathbb{R}^{\frac{W}{s} \times \frac{H}{s} \times 256}$ is then transformed into four branches: heatmap ($\hat{K} \in \mathbb{R}^{\frac{W}{s} \times \frac{H}{s} \times C}$), off-set ($\hat{O} \in \mathbb{R}^{\frac{W}{s} \times \frac{H}{s} \times 2}$), size ($\hat{S} \in \mathbb{R}^{\frac{W}{s} \times \frac{H}{s} \times 2}$) and orientation ($\hat{\theta} \in \mathbb{R}^{\frac{W}{s} \times \frac{H}{s} \times 1}$), where C is the number of classes and $s = 4$ refers to the stride. For the person detection task, $C = 1$. The output maps are gathered and decoded to generate the oriented bounding boxes of people in overhead fish-eye images.

B. Center point estimation

Given an input image $I \in \mathbb{R}^{W \times H \times 3}$, we first create a keypoint heatmap $\hat{K} \in [0, 1]^{\frac{W}{s} \times \frac{H}{s} \times C}$. Here \hat{K} is the function of x, y, c . A prediction $\hat{K}_{x,y,c} = 1$ corresponds to detected center for class c . $\hat{K}_{x,y,c} = 0$ is considered as background.

To generate ground-truth heatmaps for training, each key-point ground-truth $p \in \mathbb{R}^2$ are converted to low-resolution equivalent $\tilde{p} = \lfloor \frac{p}{s} \rfloor$. These centers are then splat using a 2D Gaussian Kernel $\exp\left(-\frac{(p_x - \tilde{p}_x)^2 + (p_y - \tilde{p}_y)^2}{2\sigma_p^2}\right)$, where σ is an object-size adaptive standard deviation [17]. The final result is the ground truth heatmap $K \in [0, 1]^{\frac{W}{s} \times \frac{H}{s} \times C}$. In case two or more Gaussians of the same class overlap, we get the element-wise maximum [23].

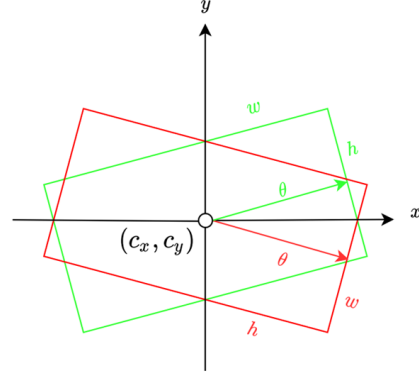


Fig. 4. Demonstration of the loss discontinuity. Given the ground truth bounding box $b_{gt} = (c_x, c_y, h, w, -1^\circ)$ and the predicted bounding box $b_{pred} = (c_x, c_y, w, h, 89^\circ)$. Due to the way rotated bounding box is represented traditionally, cost value is large even though prediction is close to ground truth.

When training the keypoint estimator, directly learning the positive center points would be difficult due to the imbalance between the positive and negative samples. To handle this problem, we decrease the penalty for the points inside the Gaussian bumps and use focal loss [24] to train the heatmap:

$$\mathcal{L}_K = \frac{-1}{N} \sum_{xyc} \begin{cases} (1 - \hat{K}_{xyc})^\alpha \log(\hat{K}_{xyc}) & \text{if } K_{xyc} = 1 \\ (1 - K_{xyc})^\beta (\hat{K}_{xyc})^\alpha & \\ \log(1 - \hat{K}_{xyc}) & \text{otherwise} \end{cases} \quad (1)$$

where N is the number of objects in image I . α and β are hyper-parameters of the focal loss. We use $\alpha = 2$ and $\beta = 4$ empirically as in [17] in all our experiments.

After the extraction of peak points from heatmaps, we have to map these coordinates to a higher dimensional input image. This will cause a discretization error as the original image pixel indices are integers and we will be predicting the float values. The offset can be calculated as $\hat{o} = (\frac{\bar{p}_x}{s} - \lfloor \frac{\bar{p}_x}{s} \rfloor, \frac{\bar{p}_y}{s} - \lfloor \frac{\bar{p}_y}{s} \rfloor)$. To predict this value, we use an offset predictor $\hat{O} \in \mathbb{R}^{\frac{W}{s} \times \frac{H}{s} \times 2}$. This offset predictor is optimized with L1 loss:

$$\mathcal{L}_{off} = \frac{1}{N} \sum_{k=1}^N |\mathbf{o}_k - \hat{\mathbf{o}}_k| \quad (2)$$

In the next section, we will show how to extend this keypoint estimator to the arbitrarily oriented person detection task.

C. Oriented bounding box regression

Let $(x_1^k, y_1^k, x_2^k, y_2^k)$ be the bounding box of object k . In addition to predicting the center point, we directly regress

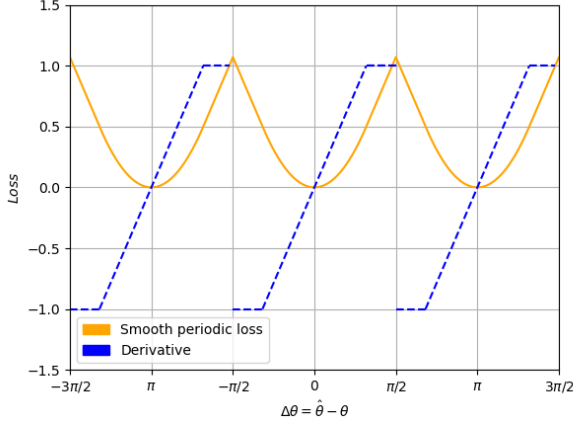


Fig. 5. Periodic loss function with smooth L1 norm and its derivative.

size $\hat{s}_k = (x_2^k - x_1^k, y_2^k - y_1^k)$ of each object. For this, we train a dimension head $\hat{S} \in \mathbb{R}^{\frac{W}{s} \times \frac{H}{s} \times 2}$ using standard L1 distance norm:

$$\mathcal{L}_{\text{size}} = \frac{1}{N} \sum_{k=1}^N |\hat{s}_k - s_k| \quad (3)$$

To capture the oriented bounding boxes, we also need to predict angle of an bounding box from it's center point. We define the orientation map as $\hat{\theta} \in \mathbb{R}^{\frac{H}{s} \times \frac{W}{s} \times 1}$. To train this orientation map, we first define the ground-truth of the orientation class. Previous works on oriented object detection often use a 5-component vector (c_x, c_y, w, h, θ) to represent the ground truth of rotated bounding boxes, where $\theta \in [-\frac{\pi}{2}, 0]$. Due to rotational symmetry, bounding box $b_1 = (c_x, c_y, w, h, \theta)$ with center points c_x, c_y , width w , height h and angle θ is indistinguishable from bounding box $b_2 = (c_x, c_y, h, w, \theta - \frac{\pi}{2})$ with width h , height w and angle $\theta - \frac{\pi}{2}$. However, common regression loss do not account for this symmetry, hence can lead to large cost even when prediction is close to ground truth (Fig. 4). We solve this by enforcing the ground truth angle θ to be in range $[-\frac{\pi}{2}, \frac{\pi}{2})$, and that w is always smaller than h . Given \hat{t}_θ as the output of the orientation map, we can compute the angle prediction as follow:

$$\hat{\theta} = \pi * \text{Tanh}(\hat{t}_\theta) \quad (4)$$

We limit the predicted angle $\hat{\theta}$ to be in range $[-\pi, \pi)$. This parametrization will later be explained in Section III-D.

D. Rotation-Aware Loss Function

Our loss function is inspired by that used in CenterNet[16], with an additional periodic loss for angle

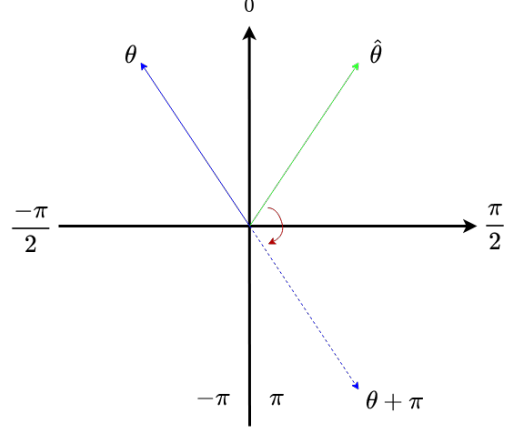


Fig. 6. In certain cases, gradient descent will cause the predicted angle $\hat{\theta}$ (green arrow) to move further away from the ground truth angle θ (blue arrow). In this case, we want the network to learn to predict $\theta + \pi$ instead of θ . To facilitate this behavior, we need to extend the angle range to include $\theta + \pi$ (dashed blue arrow) otherwise $\hat{\theta}$ will stop at $\frac{\pi}{2}$.

prediction:

$$\mathcal{L}_{\text{det}} = \mathcal{L}_K + \lambda_{\text{size}} \mathcal{L}_{\text{size}} + \lambda_{\text{off}} \mathcal{L}_{\text{off}} + \lambda_{\text{angle}} \mathcal{L}_{\text{angle}} \quad (5)$$

where $\mathcal{L}_{\text{angle}}$ is the angle loss function and $\lambda_{\text{size}}, \lambda_{\text{off}}, \lambda_{\text{angle}}$ are constants. Traditionally, common regression functions based on L1 or L2 [12], [13], [14] are used for angle prediction. However, these loss functions are not take into account the fact that since a bounding box remains identical after a rotation of $k * \pi$, the angle loss function must also satisfy that $\mathcal{L}_{\text{angle}}(\Delta\theta) = \mathcal{L}_{\text{angle}}(\Delta\theta + k\pi)$, where $\Delta\theta$ is the difference between the ground truth and the predicted angle.

To this end, we propose a new, periodic angle loss function:

$$\mathcal{L}_{\text{angle}} = \frac{1}{N} \sum_{k=1}^N \begin{cases} |\Delta\theta_{\text{periodic}}| - 0.5 & \text{if } |\Delta\theta_{\text{periodic}}| \geq 1 \\ 0.5 * \Delta\theta_{\text{periodic}}^2 & \text{otherwise} \end{cases} \quad (6)$$

where

$$\Delta\theta_{\text{periodic}} = \arctan\left(\frac{\sin \Delta\theta}{\cos \Delta\theta}\right) \quad (7)$$

Our angle loss function is π -periodic with respect to θ . The function is also defined and differentiable except for angles such as $\Delta\theta = k\pi + \frac{\pi}{2}$ (Fig. 5). We ignore these angles during backpropagation. Since ground truth angle $\theta \in [-\frac{\pi}{2}, \frac{\pi}{2})$ as stated in Section III-C, it is logical to force the predicted angle $\hat{\theta}$ to be in the same range. However, this could lead to problem for gradient descent

TABLE I. Performance comparison of ARPD with other state of the art methods on 3 fish-eye datasets. P, R and F1 denote Precision, Recall and F1-score, respectively. Results and inference speed of ARPD and RAPID is measured without any test time augmentation at confidence threshold $t_{conf} = 0.3$ using a single GTX 1070 Ti GPU. Results and FPS* of Tamura *et al.* [10] and Li *et al.* [9] are as tested in RAPID[11].

	FPS	MW				HABBOF				CEPDOF			
		AP ₅₀	P	R	F1	AP ₅₀	P	R	F1	AP ₅₀	P	R	F1
Tamura <i>et al.</i> [10]	6.8*	78.2	0.863	0.759	0.807	87.3	0.970	0.827	0.892	61.0	0.884	0.526	0.634
Li <i>et al.</i> AA [9]	0.3*	88.4	0.939	0.819	0.874	87.7	0.922	0.867	0.892	73.9	0.896	0.638	0.683
Li <i>et al.</i> AB [9]	0.2*	95.6	0.895	0.902	0.898	93.7	0.881	0.935	0.907	76.9	0.884	0.694	0.743
RAPiD [11] (608)	11.9	96.6	0.951	0.931	0.941	97.3	0.984	0.935	0.958	82.4	0.921	0.719	0.793
RAPiD [11] (1024)	6.3	96.7	0.919	0.951	0.935	98.1	0.975	0.963	0.969	85.8	0.902	0.795	0.836
ARPD (Ours)	21.2	96.1	0.935	0.906	0.92	95.6	0.968	0.927	0.947	79.8	0.889	0.702	0.784

when $\Delta\theta \in (-\frac{\pi}{2}, 0]$. When $\Delta\theta \in (-\frac{\pi}{2}, 0]$, the derivative of the angle loss function \mathcal{L}_{angle} will be negative, which will in turn cause gradient descent to move $\hat{\theta}$ away from θ (Fig. 6). Since a bounding box is identical after rotation of π , in this situation, it is preferable that the network learn to predict $\hat{\theta} + \pi$ instead. To allow this behavior, we extend the range of predicted angle $\hat{\theta}$ to $[-\pi, \pi)$. To provide steady gradients for large values of $\Delta\theta$ and less oscillations during updates when $\Delta\theta$ is small, we use smooth L1 norm for our angle loss (Fig. 5).

IV. Experimental results

A. Datasets and Implemetation details

We evaluate our method on three publicly available fish-eye datasets: Mirror World (MW) [19], HABBOF [9] and CEPDOF [11]. All three datasets contain videos of people captured by ceiling-mounted fish-eye cameras in various scenarios. Further information about the datasets are given in Table II. To measure the performance of our algorithm, we adopt the Average Precision metric used by COCO [25] in addition to F1 score, precision and recall. Since a single person can be represented by multiple ground-truth rotated bounding boxes with different angles, we only consider the AP at IoU = 0.5 (AP₅₀). We use a confidence threshold of 0.3 for all our tests.

For the training and testing stage, we resize the input image to 512×512 . In addition to random flip, random cropping, random scaling, and color jittering, we also use random rotation augmentation. We first train our network on MS COCO 2017 [25] for 90 epochs. In the training phase, perspective images (containing people) from the COCO dataset are randomly rotated before being input into the network. We split the three datasets into train/test split, i.e., two datasets are used for training, and the remaining are used for testing. For example, we fine-tune ARPD on HABBOF and CEPDOF for 10 epochs, and test it on MW. This process is repeated for all permutations. We use Adam optimizer with an initial learning rate of 1.25×10^{-4} , with learning rate drop at

TABLE II. Statistics of three publicly available overhead fish-eye image datasets. All images have a 360° field of view and 1:1 aspect ratio.

Dataset	# of videos	# of frames	# of GT boxes
MW	19	8752	22758
CEPDOF	4	25504	173428
HABBOF	8	5873	20430

epochs 60 and 80. Unless otherwise specified, we set $\lambda_{off} = 1$ and $\lambda_{size} = \lambda_{angle} = 0.1$ in all of our experiments. We train the network with the batch size of 32 on two NVIDIA 2080Ti. The inference speed is measured on a single NVIDIA 1070Ti.

B. Main results

Results from Table. I shows that ARPD’s performance come close to the top-performing algorithm, while running many times faster than all other methods tested. This makes ARPD superior for the real-time person detection task. Our method outperforms Tamura *et al.*’s method [10] by a considerable margin on all three fish-eye datasets, and is slightly better in terms of AP compared to the method of Li *et al.* [9], while running tens of times faster. We achieve an execution speed of 21 frames per second, which is nearly two times faster than RAPID while not having to sacrifice considerably in terms of accuracy. ARPD achieves an AP₅₀ score of more than 95 on MW and HABBOF, both of which mostly consist of people walking and standing appearing radially-oriented (Fig. 7 a-e). ARPD is also capable of detecting various challenging scenarios in CEPDOF such as extreme body poses or occlusion (Fig. 7 f-g). However, scenarios such as low-light or small objects remain difficult (Fig. 7 h).

C. Ablation Experiments

In this section, we conduct various experiments to analyze how individual parts of ARPD contributes to the overall performance, and the effectiveness of novel

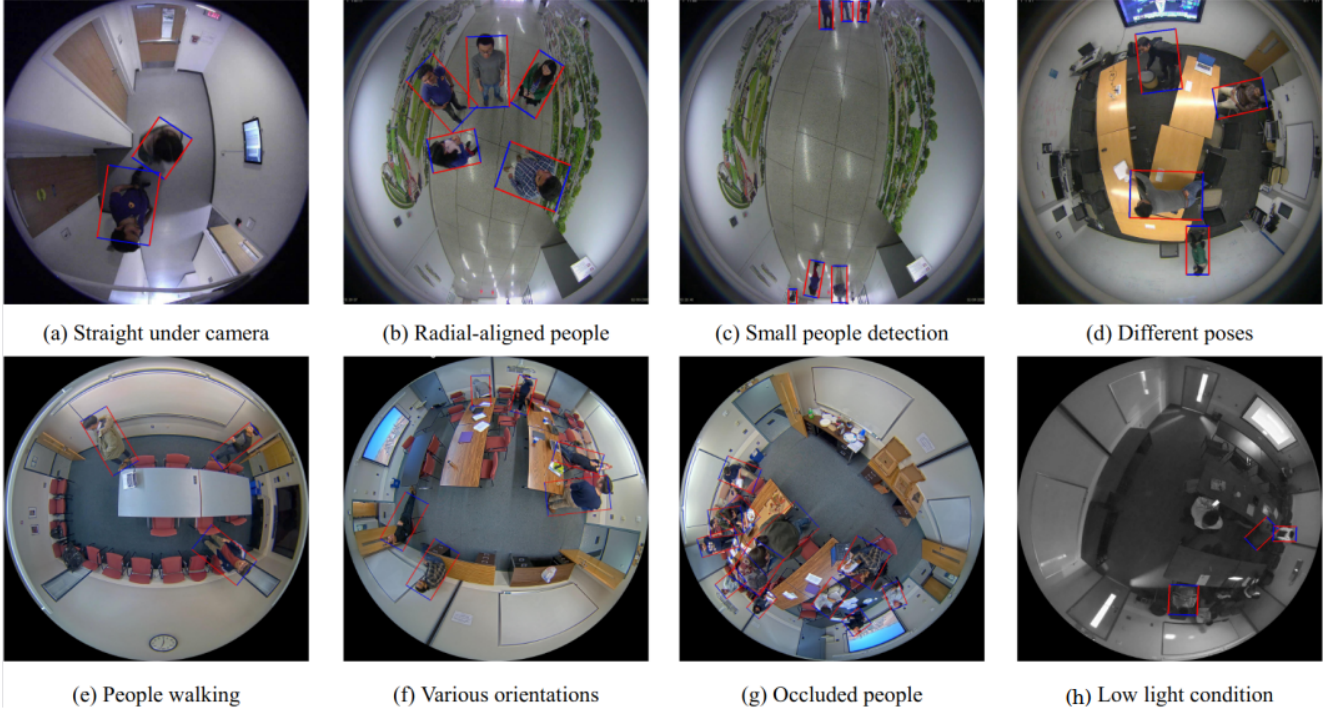


Fig. 7. Qualitative results of ARPD on MW (a-d), HABBOF (e) and CEPDOF (f-h). ARPD works well on both easy and challenging cases, such as heavy occlusion, various poses and background. For cases of small people detection (c), in some cases the bounding boxes does not fully enclose the person. Unsurprisingly, low-light scenarios (h) remains challenging.

TABLE III. Ablation experiments conducted on Mirror World dataset. Results are shown in COCO AP_{50} .

Method		ARPD						
Angle loss	L1	✓						
	Periodic L1		✓					
	Smooth periodic L1			✓	✓	✓	✓	✓
Prediction range	$[-\frac{\pi}{2}, \frac{\pi}{2})$	✓	✓	✓				
	$(-\infty, \infty)$				✓			
	$[-\pi, \pi)$					✓	✓	✓
λ_{angle}	1	✓	✓	✓	✓	✓		
	0.01						✓	
	0.1							✓
AP_{50}		86.2	88.9	90.1	92.1	93.2	95.3	96.1

elements we introduced.

Rotation aware Angle loss: We compare the performance of our novel periodic loss function against commonly used regression loss functions. Results from Table III proves that our loss function is better for oriented person detection. Smooth L1 norm also performs slightly better than L1. This can be explained due to the fact that Smooth L1 allows for better optimization when $\Delta\theta$ is small.

Parameterization of oriented bounding box: As shown in Table III, there is a notable performance improvement when we extend the prediction range from

$[-\frac{\pi}{2}, \frac{\pi}{2})$ to $[-\pi, \pi)$, however increasing it further does not significantly impact accuracy.

Impact of different orientation weight: We test the approach’s sensitivity to the orientation weight λ_{angle} . $\lambda_{angle} = 0.1$ yields the best result. Performance noticeably deteriorate when $\lambda_{angle} > 0.1$.

V. Conclusions

In this paper, we propose ARPD, a new oriented person detection method in fish-eye images based on center point detection. ARPD is single-stage, free of anchor or NMS post-processing. In addition to the location and dimension of the bounding boxes, ARPD

also predicts its angle of rotation. We also introduce an angle-aware periodic loss function based on smooth L1 norm, which considers angle periodicity and is more sensitive towards small-angle variation between ground truth and prediction. Experimental results show that our method achieves the best speed-to-accuracy trade-off on multiple fish-eye datasets. Our method would benefit real-world applications and serve as a baseline algorithm for real-time person detection on fish-eye cameras.

References

- [1] J. Redmon, S. Divvala, R. Girshick, and A. Farhadi, "You only look once: Unified, real-time object detection," in *Proceedings of the IEEE conference on computer vision and pattern recognition*, pp. 779–788, 2016. 1, 2
- [2] W. Liu, D. Anguelov, D. Erhan, C. Szegedy, S. Reed, C.-Y. Fu, and A. C. Berg, "Ssd: Single shot multibox detector," in *European conference on computer vision*, pp. 21–37, Springer, 2016. 1, 2
- [3] S. Ren, K. He, R. Girshick, and J. Sun, "Faster r-cnn: Towards real-time object detection with region proposal networks," *Advances in neural information processing systems*, vol. 28, pp. 91–99, 2015. 1, 2
- [4] Y.-W. Choi, K.-K. Kwon, J.-H. Kim, K.-J. Na, and S.-G. Lee, "Real time omni-directional object detection using background subtraction of fisheye image," *Journal of Institute of Control, Robotics and Systems*, vol. 21, no. 8, pp. 766–772, 2015. 1, 3
- [5] E. Bas, D. Erdogmus, U. Ozertem, and M. Pavel, "Towards fish-eye camera based in-home activity assessment," in *2008 30th Annual International Conference of the IEEE Engineering in Medicine and Biology Society*, pp. 2558–2561, IEEE, 2008. 1, 3
- [6] P. Dollár, R. Appel, S. Belongie, and P. Perona, "Fast feature pyramids for object detection," *IEEE transactions on pattern analysis and machine intelligence*, vol. 36, no. 8, pp. 1532–1545, 2014. 2, 3
- [7] A.-T. Chiang and Y. Wang, "Human detection in fish-eye images using hog-based detectors over rotated windows," in *2014 IEEE International Conference on Multimedia and Expo Workshops (ICMEW)*, pp. 1–6, IEEE, 2014. 2, 3
- [8] O. Krams and N. Kiryati, "People detection in top-view fisheye imaging," in *2017 14th IEEE international conference on advanced video and signal based surveillance (AVSS)*, pp. 1–6, IEEE, 2017. 2, 3
- [9] S. Li, M. O. Tezcan, P. Ishwar, and J. Konrad, "Supervised people counting using an overhead fisheye camera," in *2019 16th IEEE International Conference on Advanced Video and Signal Based Surveillance (AVSS)*, pp. 1–8, IEEE, 2019. 2, 3, 6
- [10] M. Tamura, S. Horiguchi, and T. Murakami, "Omnidirectional pedestrian detection by rotation invariant training," in *2019 IEEE winter conference on applications of computer vision (WACV)*, pp. 1989–1998, IEEE, 2019. 2, 3, 6
- [11] Z. Duan, O. Tezcan, H. Nakamura, P. Ishwar, and J. Konrad, "Rapid: rotation-aware people detection in overhead fisheye images," in *Proceedings of the IEEE/CVF Conference on Computer Vision and Pattern Recognition Workshops*, pp. 636–637, 2020. 2, 3, 6
- [12] X. Yang, H. Sun, K. Fu, J. Yang, X. Sun, M. Yan, and Z. Guo, "Automatic ship detection in remote sensing images from google earth of complex scenes based on multiscale rotation dense feature pyramid networks," *Remote Sensing*, vol. 10, no. 1, p. 132, 2018. 2, 3, 5
- [13] J. Ding, N. Xue, Y. Long, G.-S. Xia, and Q. Lu, "Learning roi transformer for detecting oriented objects in aerial images," *arXiv preprint arXiv:1812.00155*, 2018. 2, 3, 5
- [14] X. Yang, Q. Liu, J. Yan, A. Li, Z. Zhang, and G. Yu, "R3det: Refined single-stage detector with feature refinement for rotating object," *arXiv preprint arXiv:1908.05612*, vol. 2, no. 4, 2019. 2, 3, 5
- [15] K. Duan, S. Bai, L. Xie, H. Qi, Q. Huang, and Q. Tian, "Centernet: Keypoint triplets for object detection," in *Proceedings of the IEEE/CVF International Conference on Computer Vision*, pp. 6569–6578, 2019. 2
- [16] X. Zhou, D. Wang, and P. Krähenbühl, "Objects as points," *arXiv preprint arXiv:1904.07850*, 2019. 2, 3, 4, 5
- [17] H. Law and J. Deng, "Cornersnet: Detecting objects as paired keypoints," in *Proceedings of the European conference on computer vision (ECCV)*, pp. 734–750, 2018. 2, 4
- [18] X. Zhou, J. Zhuo, and P. Krahenbuhl, "Bottom-up object detection by grouping extreme and center points," in *Proceedings of the IEEE/CVF Conference on Computer Vision and Pattern Recognition*, pp. 850–859, 2019. 2
- [19] N. Ma, "Mirror worlds challenge." Retrieved from <http://www2.icat.vt.edu/mirrorworlds/challenge/index.html>. 2, 6
- [20] F. Yu, D. Wang, E. Shelhamer, and T. Darrell, "Deep layer aggregation," in *Proceedings of the IEEE conference on computer vision and pattern recognition*, pp. 2403–2412, 2018. 3
- [21] R. Girshick, "Fast r-cnn," in *Proceedings of the IEEE international conference on computer vision*, pp. 1440–1448, 2015. 2
- [22] R. Girshick, J. Donahue, T. Darrell, and J. Malik, "Rich feature hierarchies for accurate object detection and semantic segmentation," in *Proceedings of the IEEE conference on computer vision and pattern recognition*, pp. 580–587, 2014. 2
- [23] Z. Cao, G. Hidalgo, T. Simon, S.-E. Wei, and Y. Sheikh, "Openpose: realtime multi-person 2d pose estimation using part affinity fields," *IEEE transactions on pattern analysis and machine intelligence*, vol. 43, no. 1, pp. 172–186, 2019. 4
- [24] T.-Y. Lin, P. Goyal, R. Girshick, K. He, and P. Dollár, "Focal loss for dense object detection," in *Proceedings of the IEEE international conference on computer vision*, pp. 2980–2988, 2017. 4
- [25] T.-Y. Lin, M. Maire, S. Belongie, J. Hays, P. Perona, D. Ramanan, P. Dollár, and C. L. Zitnick, "Microsoft coco: Common objects in context," in *European conference on computer vision*, pp. 740–755, Springer, 2014. 6